Shifting paradigms in Ocean Color: Bayesian Inference for Uncertainty-Aware Chlorophyll Estimation

Erdem M. Karaköylü[1], **Susanne E. Craig**[2]

[1]Independent Researcher,
[2]NASA/UMBC,

Corresponding author: Erdem M. Karaköylü, erdemk@protonmail.com

Abstract
Placeholder

Plain Language Summary
Placeholder

1 Introduction

Satellite ocean color remote sensing has long served as a cornerstone of marine ecosystem monitoring, offering global and synoptic coverage of surface ocean properties. Among these, chlorophyll-a (Chl_a) concentration remains a central metric, widely used as a proxy for phytoplankton biomass, primary production, and water quality. The retrieval of Chl_a from ocean color data has evolved over decades, resulting in a diverse lineage of empirical and semi-empirical algorithms. The following section summarizes this historical development, which sets the stage for a critical examination of the statistical foundations underlying current approaches.

1.1 Historical Context of Chlorophyll Algorithms

Satellite ocean color observations have long been fundamental for monitoring marine ecosystems, as they enable global estimation of chlorophyll-a (Chl_a) — a key indicator of phytoplankton biomass and ocean productivity. Early empirical algorithms, notably developed by O'Reilly et al. (John E. O'Reilly et al., 1998; John E. O'Reilly et al., 2000), established the OCx family (where x denotes the number of bands used) of polynomial regression models. These models relate blue-to-green reflectance ratios (after log-transformation) to in situ Chl_a, employing either straight band ratios (BR) or maximum band ratios (MBR)—the latter selecting the highest available blue-to-green ratio for any given observation as input to a high-order polynomial. These formulations have served as the operational foundation for chlorophyll-a products across a broad range of satellite ocean color sensors—from the pioneering Coastal Zone Color Scanner (CZCS) through SeaWiFS, MODIS, and MERIS to more recent missions—offering a straightforward and robust approach for Case-1 waters. However, their performance is more limited in optically complex Case-2 waters and remains sensitive to atmospheric correction errors.

Subsequent refinements were introduced to address these deficiencies. For example, Hu et al. (Hu et al., 2012) proposed a Color Index (CI) formulation that employs a band-difference approach to reduce sensitivity to residual atmospheric errors and instrument noise, with further improvements enhancing inter-sensor agreement (Hu et al., 2019). The increasing availability of calibration data (e.g., (**Valente2015?**)) and ongoing algorithmic improvements have led to the development of additional variants of the OCx algorithms—specifically, the OC5 and OC6 formulations. O'Reilly and Werdell (John E. O'Reilly & Werdell, 2019) maintain that OC5 extends the spectral basis by incorporating the 412 nm band, thereby exploiting its strong signal in clear, oligotrophic waters, while OC6 replaces the traditional denominator with the mean of the 555 and 670 nm reflectances, with the aim of improving the dynamic range at low chlorophyll concentrations. In total, (John E. O'Reilly & Werdell, 2019) propose 65 versions of BR/MBR OCx type algorithms for 25 sensors—on average, two or more variants per sensor. With this arsenal, it is hoped, researchers are better equipped to address the wide array of bio-optical environments encountered in global ocean color applications.

1.2 Limitations of Existing Approaches

Regrettably, the development of traditional ocean color algorithms is grounded in a fundamental statistical error—one that pervades much of observational science: the conflation of sampling probability with inferential probability (Jaynes & Bretthorst, 2003; **DeScheemaekere2011?**).

Consider a dataset D composed of input–output pairs—e.g., remote sensing reflectance (Rrs) and chlorophyll-a concentration (Chl_a)—and a model M, such as OCx, posited to represent the relationship between them. The sampling probability $p(D \mid M)$ denotes the probability of observing data D under the assumption that model M is true. In standard model fitting, this likelihood is maximized by adjusting the parameters of M to best explain the observed data.

This approach tacitly assumes that the model which best fits the data also most accurately represents the underlying generative process. This constitutes an epistemic fallacy—treating $p(D \mid M)$ as if it were $p(M \mid D)$—a direct violation of Bayes' theorem and the rules governing conditional probability.

Although in well-behaved, data-rich cases—where the likelihood is regular, the signal strong, and the model adequately constrained—the maxima of $p(D \mid M)$ and $p(M \mid D)$ may coincide, this remains the exception—not the rule.

This mistake lies at the heart of what Clayton (Clayton, 2022) terms the Bernoulli Fallacy: the widespread misinterpretation of likelihood as inference, or of data-fit as belief. As Clayton argues, this logical misstep has far-reaching consequences, with implications that extend beyond science to domains such as medicine, law, and public policy.

In scientific modeling, this fallacy contributes to poor generalization, drives the use of ad hoc or retrospective uncertainty quantification, and underlies many published results that later prove difficult to replicate (Baker, 2016; Cobey et al., 2024). These limitations are not restricted to classical hypothesis testing; they persist in the training and deployment of modern machine learning models as well.

In regression and classification, maximizing likelihood is often treated as sufficient for inference—despite yielding only a single point estimate and ignoring both parameter uncertainty and the plausibility of alternative models.

This epistemic shortcut has been directly critiqued in the machine learning literature. Gal (Gal, 2016) and Ghahramani (**gahramani2015probabilistic?**) point out that most ML models discard uncertainty altogether, treating the outcome of an optimization as if it were an inference. The result is overconfident predictions and brittle generalization—concerns that echo Clayton's critique.

Bishop (Bishop, 2006) similarly distinguishes between the utility of predictive models and the inferential scaffolding required to quantify uncertainty, reinforcing the notion that likelihood alone is insufficient—and that the Bernoulli Fallacy permeates much of applied machine learning.

1.3 Overcoming limitations

Several recent efforts have attempted to address the limitations of classical retrieval models. For instance, (Seegers et al., 2018) proposed alternative evaluation metrics to move beyond restrictive frequentist assumptions. Others have incorporated Bayesian elements into the modeling pipeline: (Frouin & Pelletier, 2013) applied Bayesian inversion for atmospheric correction, (**shi2015?**) used probabilistic fusion for multi-sensor data, and (Craig & Karaköylü, 2019) employed Hamiltonian Monte Carlo to train Bayesian neural networks (BNNs) for retrieving inherent optical properties (IOPs) from top-of-atmosphere radiance. Similarly, (**werther2022?**) introduced Monte Carlo dropout as an approximate BNN strategy, while (Erickson et al., 2023) recast the Generalized Inherent Optical Property (GIOP) framework using conjugate Bayesian linear models. Most recently, (**hammout2024?**) developed a BNN surrogate using stochastic variational inference for chlorophyll-a prediction from Rrs.

While these studies mark important progress, they often adopt only isolated components of what has come to be known as the Bayesian workflow (**bgelman2019?**).

Key aspects—such as principled prior specification, posterior predictive checking, and formal model comparison—remain largely absent. As a result, uncertainty is frequently approximated rather than inferred, and model structure is rarely treated as a variable to be interrogated.

This paper builds on prior work and extends it by applying a fully Bayesian modeling framework for chlorophyll-a prediction from sea surface reflectance (Rrs), with explicit treatment of uncertainty, model complexity, and measurement error.

2 Materials and Methods

This section outlines the dataset, model structures, inference methods, and model evaluation criteria used in this study. I focus on a fully Bayesian approach to modeling chlorophyll-a from satellite remote sensing reflectance (Rrs), emphasizing transparency, uncertainty quantification, and principled model comparison. Four models are presented in the main text, while all six model formulations and results are included in the Supplement.

2.1 Data Description and Preparation Overview

For pedagogical reasons, I used the well known NOMAD (Werdell & Bailey, 2005) dataset, which includes quality-controlled in situ measurements of chlorophyll-a matched with coincident satellite Rrs data. These measurements span a range of oceanographic conditions, enabling the development of models that are expected to generalize across water types. The data were loaded using the Python Pandas library (team, 2020), which was used for all subsequent cleaning, preprocessing, and transformation operations.

Raw Data - Sea-surface reflectances (Rrs) in the 6 visible SeaWiFS bands (411, 443, 489, 510, 550, 670nm) constitue the bulk of the data. Chlorophyll concentrations, measured via fluorescence or HPLC or both, consituted the target variables. Any row containing an invalid data point (null, zero, or negative) was removed, as proper missing/invalid data imputation is a subject onto itself and beyond the scope of this paper.

Data Preprocessing and Transformation - Chlorophyll measurements from the two different methods were combined into a single data. An auxiliary column was used to flag the measurement method as 'fluo' of 'hplc'. The chlorophyll was then log-transformed to stabilize its variance. The max band ratio (MBR) was computed as $\frac{\max(Rrs411, Rrs443, Rrs489, Rrs)}{Rrs555+Rrs670}$, similar to the OC6 model proposed by (John E. O'Reilly & Werdell, 2019). Another ancillary column was created to captured the actual Rrs band used for each set observations. This numerator type as well as the chlorophyll measurement type are useful to build more hierarchical partial pooling models that can take advantage of such data groups. A sample from the fully processed data used in the subsequent models can be seen in (**data-table?**).

	log_MBR	MBR_flag	log_chl	hplc_flag
905	-0.2545615131431814	Rrs510	0.5837653682849998	hplc
91	-0.3641327253450254	Rrs510	1.0511525224473812	fluo
528	-0.0737170739918758	Rrs510	0.14363923527454328	fluo
969	0.5813600497877703	Rrs411	-0.8272803386505035	fluo
552	0.7134341855521412	Rrs443	-0.9318141382538383	hplc

A random 5-row sample from the Pandas dataframe holding the data used in subsequent models. *log_MBR* is the log-transformed Max. Band Ratio (MBR) of sea surface reflectances, where the numerator is Max(Rrs411, Rrs443, Rrs489, Rrs510) and the denominator is computed from the sum of Rrs555 and Rrs670. *MBR_flag*

indicates which of the 4 possible Rrs bands is used in the numerator for that particular row. *log_chl* is log transformed in-situ measured chlorophyll *a* concentration, originally in $mg\ m^{-3}$. *hplc_flag* is a binary variable indicating whether the measurement was obtained via HPLC or fluorometry. "-flag" are used during modeling for grouping data for hierarchical partial pooling models, explained further below. These groupings can be seen in Figure 1

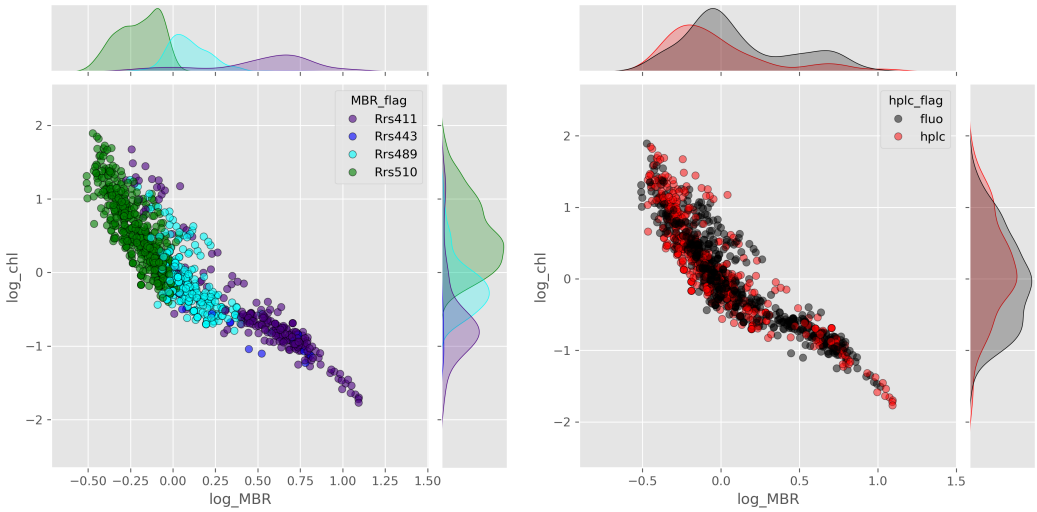

(a) (b)

Figure 1: Two ways of grouping the data. Figure 1a, max band ratio numerator; Figure 1b, chlorophyll measurement method.

2.2 Bayesian Modeling Framework

Several models of increasing levels were built. All models use $log(MBR)$ as primary input and $log(chl)$ as target, some use MBR_flag as additional input, the last model also uses $hlpc_flag$. The following are key components shared across models.

Likelihood - A truncated gaussian distribution with support constrained to -3.0 to 3.2 on the log_{10} scale,corresponding to $0.001 - 1600 mg\ m^{-3}$ to reflect both detectable realistic levels of marine surface chlorophyll.

Noise Structure - Noise was incorporated as likelihood dispersion parameter σ; some of the models use a constant σ, others take heteroscedasticity into account.

Priors - To estimate model posterior distribution, and produce predictions with uncertainty following data fitting, all model parameters receive a prior distribution, making explicit model assumptions. Often there will be enough data to overrule the priors, which are here mostly a conduit to the Posterior. An important caveat is that care should be taken not to assign a 0-probability through a poorly specified prior where support might actually be needed. Less importantly, more efficient use of the search space can be done through priors that assign 0-probability where support is clearly unreasonable. Thus, all regression parameters receive Normal (Gaussian) 0-centered weakly informative priors. And all σ terms received Gamma priors that provide flexible but strictly positive support.

Software - All models were implemented with the Python probabilistic programming library PyMC V.5 (Abril-Pla et al., 2023) and estimated using a variant of Hamil-

tonian Monte Carlo known as the No-U-Turn Sampler (NUTS). Model diagnostics inference evaluation and model comparisons were done through the Arviz package.

2.3 Overview of Candidate Models

I developed six models representing a progression of modeling complexity and assumptions:

- **Model 1**: Polynomial regression (Bayesian OC6-style baseline)
- **Model 2**: Hierarchical linear regression, grouped by dominant MBR numerator band
- **Model 3**: Similart to Model 2, with group-specific constant likelihood variance
- **Model 4**: Global linear heteroscedastic model
- **Model 5**: Similar to Model 2, with group-wise linear heteroscedasticity
- **Model 6**: Model 6 plus an added dispersion term for fluorescence-based measurements

The main text focuses on Models 1, 2, 5, and 6, which span the range of key structural variations. Full equations, priors, and diagnostic results for all models are provided in the Supplement.

2.4 Representative Model Structures

Models are described here as sets of equations and Directed Acyclic Graphs (DAG), with the former providing numerical details while the latters helps visualize model structure and flow.

2.4.1 Model 1: Bayesian 4th Order Polynomia Regression

This model follows the OC6 formulation proposed by O'Reilly et al. (2019), with the difference that the denominator is the sum of $Rrs555$ and $Rrs670$ rather than the mean. The model mean is a fourth-order polynomial of $log(MBR)$ to estimate $log(Chl)$. The set of proabilistic equations that define this model can be found in the Supplemental Material Section. The model structure and inference flow is represented in Figure 2 as a Directed Acyclic Graph (DAG).

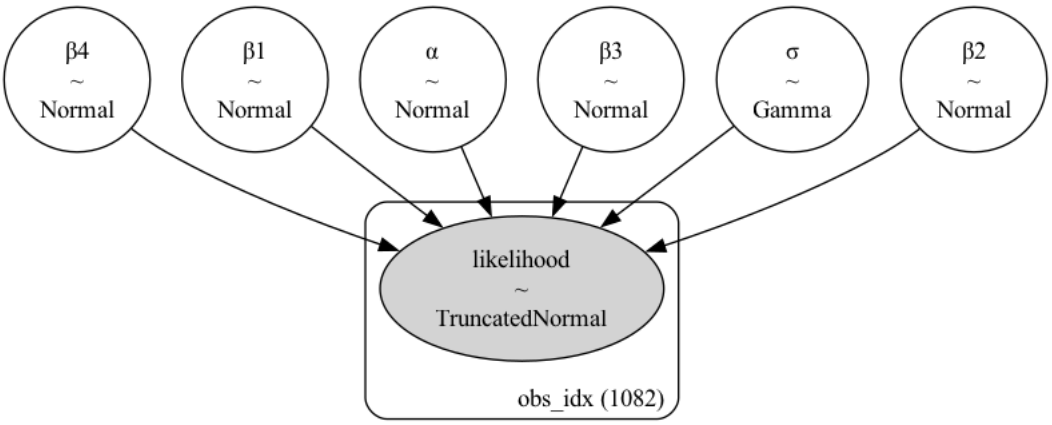

Figure 2: Model 1 Directed Acyclic Graph showing model parameters and their prior distributions and how they relate . The intercept α and the polynomial slopes, β1-β4 all have Gaussian priors; σ, the likelihood dispersion parameter, receives a Gamma prior; the likelihood itself is constrained by a Truncated Normal distribution (see text for more). The plate containing the likelihood is indexed (obs_idx) indicating the likelihood will be computed for each of the 1082 observations available.

2.4.2 Model 2: Hierarchical Linear Regression (HLR)

Model 2 introduces partial pooling across four groups defined by the dominant MBR numerator band; Rrs411, Rrs443, Rrs489, Rrs510 (*cf.* Figure 1a). Each group receives its own slope and intercept, and these parameters have shared hyperpriors. Consequently, each group has its own sub-model that can capture details specific to it and the shared hyperpriors allow for the sharing of information between groups when fitting the model. This approach maximizes the use of information contained in the available data. Hierarchical models are usually result in uncertainty shrinkage. Mathematical description of the model can be found in the Supplementary Material. Figure 3 illustrates the model structure.

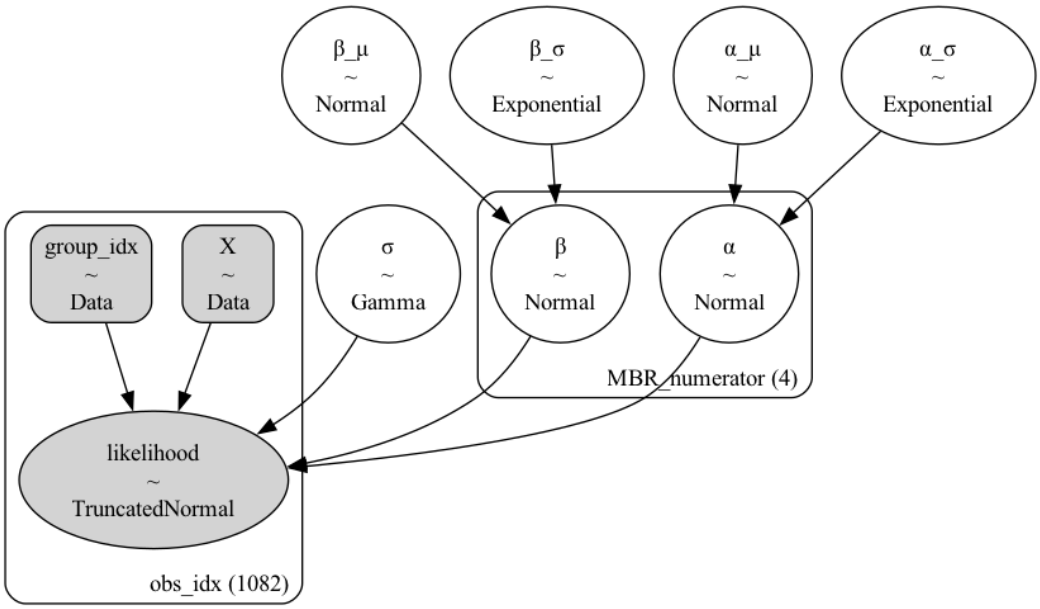

Figure 3

2.4.3 Model 5: HLR with Added Linear Heteroscedastic Likelihood Dispersion

The data plotted in Figure 1 suggests heteroscedasticity - variance that is not constant, but rather changes depending on the data. Models 3 and 4 investigate the role of group-wise constant heteroscedasticity and global linear heteroscedasticity, respectively. Details of these models can be found in the Supplementary Material section. To investigate this further, Model 5 looks at group-wise linear heteroscedasticity. Thus, for a given MBR group j σ_j is modeled as a log-linear relationship such that $log(\sigma) = \alpha_j + \beta_j \times log(MBR)$ and then transformed via $exp(log(\sigma_j))$ before being passed on to the likelihood. Similar to the model mean, μ_j, σ_j's slope and intercept terms are partially pooled and so have common hyperpriors. Mathematical description of the model can be found in the Supplementary Material section; Figure 4. illustrates the model structure.

2.4.4 Model 6: Augmenting Model 5 with Measurement-Specific Dispersion

A reasonable assumption is that HPLC measurements are less noisy than fluorescence. This model adds a measurement-method-specific dispersion term to the structure of Model 6, to capture the suspected increase in variability associated with fluorescence-based chlorophyll estimates. The likelihood dispersion, σ, is given the

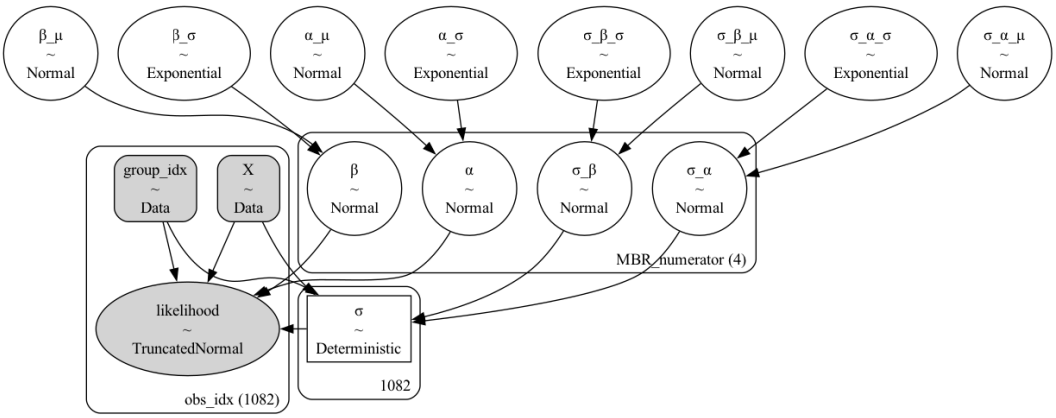

Figure 4

expression $log(\sigma) = \alpha_j + \beta_j \times log(MBR) + \gamma_{chl\_type} * (1 - chl_{type\_idx})$, where $chl_{type\_idx} = 1$ if *in-situ* chlorophyll was measured with HPLC, 0 otherwise. As a result, σ is the same as in Model 5 if $chl_{type\_idx} = 1$, since the extra term is nullified. In the case of fluorescence measurement, on the other hand, $log(\sigma)$ receives an extra noise term, providing an effective measurement of noise difference between the two methods. Figure 5 shows the inference DAG of Model 6.

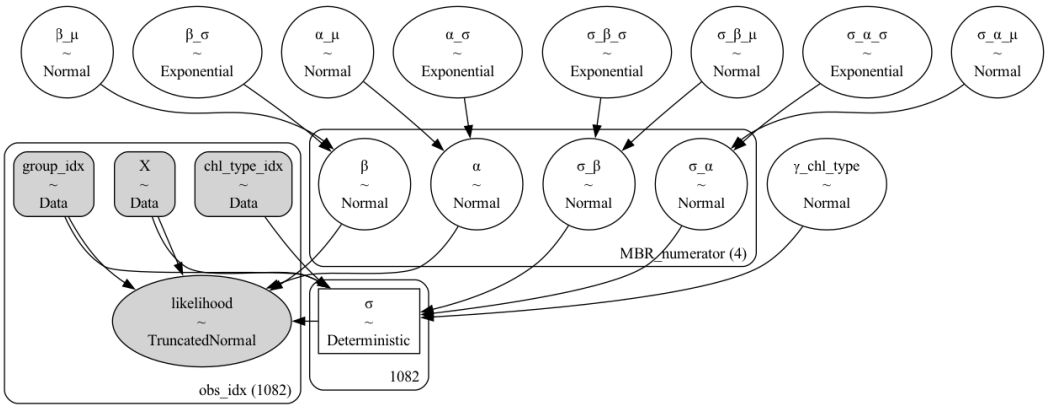

Figure 5: Model 6 - Similar to Model 5; multi-level hierarchical linear model partial pooling across MBR groups (Rrs411, Rrs443, Rrs489, Rrs510) for both model mean and variance. However the linear variance model gets an additional parameter γ that allows for the model dispersion to depend on the chlorophyll measurement method (fluorescence or HPLC). While this does not necessarily affect future , for which ground truth mearuement are optional, it does allow the development of insight on the effect of chloroophyll measurement method on model ucertainty.

2.5 Prior Specifications and Model Fitting

Priors - I used weakly informative priors across all models to balance flexibility with regularization. For regression parameters I used Gaussian priors, In the case of the single-level Model 1, this meant priors with 0 mean and variance of 1 to encourage parameter sparsity. In the case of Models 2-6, which are multi-level models, hy-

perpriors of prior means were set to Gaussans of mean 0 and variance 1, again to encourage sparsity. Variance hyperpriors were given Exponential distributions with rate set to 1 with significant density near 0, whichß encourages similarity across groups unless the data mandates otherwise. This hyperprior also encourages uncertainty shrinkage across groups if possible. In the case of homoscedasticity, or group-wise heteroscedasticity, I used a Gamma prior of shape and scale of 2 for the likelihood dispersion σ, which provides strictly postivie support. Prior soundness was assessed using *Prior Predictive Checks*. This procedure takes advantage of the fact taht Bayesian models are generative, meaning the model can be sampled without data, to insure that values of $(log(Chl))$ predicted by the model are reasonable even before model fitting. Prior predictive $log(Chl)$ values were plotted as Cumulative Distribution Function (CDF) of $log(Chl)$. Figure 6 shows such a plot for Model 1.

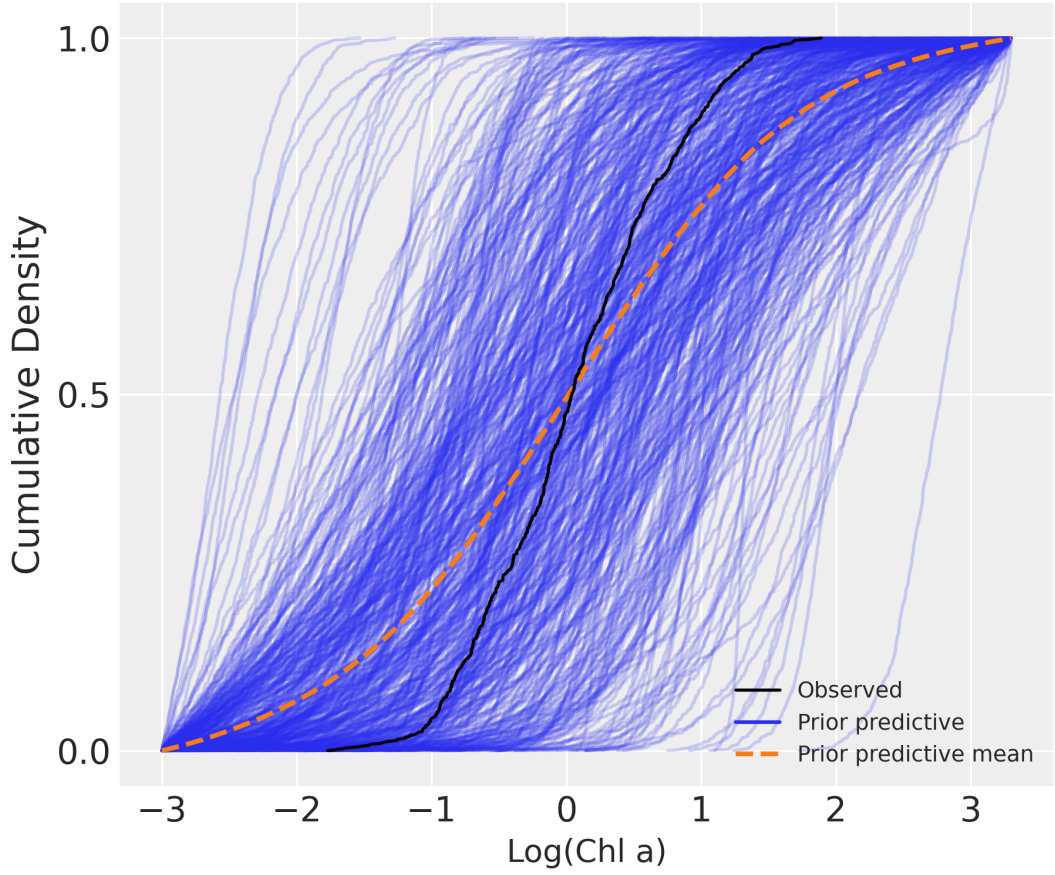

Figure 6: Prior Predictive Checks, here shown for Model 1. This step allows the practitioner to verify the soundness of model assumptions - choice of priors, the model formulation, etc. This can be done even before data is collected as the generative nature of Bayesian models means output can be produce based solely on the priors and the model's mathematical expression alone. Results are presented as Cumulative Distribution Function. In blue, 500 draws were performed each containing a prescribed number of observations. The dashed line represents the CDF of the simulation mean, In black, the CDF of the data is shown for comparison.

See *Results* section for a Prior Predictive Checks plot example; plots for all models can be found in the Supplementary Material section.

Model Fitting - The model posterior was approximated using the No U-Turn Sampler (NUTS), an efficient and mature variant of Hamiltonian Monte Carlo (HMC), which uses particle physics to sample the posterior; see the Supplementary Materials section for more details. Sampler settings were as follows. Four independent sampling runs referred to as *chains* were used to assess sampler convergence. Prior to sampling, 1000 tuning steps were used for each chain to maximize sampler efficiency. The 2000 samples were recorded for each chain totalling 8000 samples. I assessed sampler convergence using the Gelman-Rubin statistic, $\hat{R}$ and effective sample size(ESS). Convergence is acceptable for $\hat{R} < 1.01$ and $ESS > 1000$. Full trace plots and diagnostics are included in the Supplementary Material section. Goodness of fit was assessed using *Posterior plots*, which show *Posterior Predictive Checks, which show the expected

2.6 Model Comparison and Predictive Evaluation

I compared model performance using **Pareto Smoothed Importance Sampling Leave-One-Out Cross-Validation (PSIS-LOO-CV)** (Vehtari et al., 2017). This Bayesian metric estimates the expected log predictive density (ELPD), a principled measure of out-of-sample predictive accuracy, that uses the entire posterior predictive distribution

- Models were ranked by ELPD
- ΔELPD values were interpreted relative to their standard errors
- Pareto-k diagnostics confirmed LOO reliability (full table in Supplement)

I evaluated predictive accuracy and calibration using:

- **Posterior Predictive Checks (PPCs)**:
  - Simulated draws overlaid on observed distributions
  - Empirical CDF comparisons and interval coverage
- **HDI coverage**:
  - Fraction of observed values falling within 95% posterior predictive intervals

No frequentist evaluation criteria such as RMSE, MAE, or R^2 were used at any stage as these do not make sense in this context where for each observations, a probability distribution of the prediction is produced.

3 Results

This section presents the outputs of posterior inference, model comparison using Bayesian criteria, and posterior predictive diagnostics for the four primary models. Results from the three supplementary models are provided separately in the Supplement.

3.1 MCMC Convergence

All four models converged successfully. The Gelman-Rubin statistic (R-hat 1.0) and large effective sample sizes (ESS > 1000) across all parameters indicate robust posterior estimation. Diagnostic plots and sampling traces are provided in the Supplementary Material.

- All R-hat < 1.01
- No divergences
- Sufficient tail and bulk ESS
- Full diagnostics in Supplement

3.2 Predictive Performance via Leave-One-Out Cross Validation

We compared models using Pareto Smoothed Importance Sampling Leave-One-Out Cross-Validation (PSIS-LOO-CV), a fully Bayesian approach to evaluating out-of-sample predictive accuracy.

Table 1. Leave-One-Out Comparison (ELPD ± SE):

- Model 7 ranked highest in expected log predictive density (ELPD)
- Model 6 performed comparably, with ΔELPD within 1 SE
- Model 1 (OC6 polynomial) had the weakest predictive performance
- All models had acceptable Pareto-k diagnostics (see Supplement)

3.3 3.3 Posterior Predictive Checks (PPC)

We used posterior predictive checks (PPCs) to evaluate the ability of each model to reproduce key features of the observed log-chlorophyll distribution. These include:

- Empirical CDF comparisons
- HDI envelopes overlaid on the data
- Predictive median vs. observed values

Figure 1. Posterior predictive envelopes vs. observed log(Chl)
Figure 2. ECDF overlays with posterior predictive means and HDIs
Figure 3. Rug plot of observations with overlaid posterior predictive draws

Findings: - Model 7 captures full data distribution, especially for fluorescence-labeled values - Model 1 underestimates tails (under-dispersed) - Model 6 accurately reflects group-level variance

3.4 3.4 Posterior Distributions and Interpretability

Posterior distributions for key parameters illustrate how model structure affects inference. We show both: - Group-level slopes and intercepts (hierarchical structure) - Group-wise (heteroscedasticity) - Fluorescence-specific variance term (Model 7)

Figure 4. Forest plot of slope and intercept posteriors
Figure 5. Posterior of across MBR groups
Figure 6. Posterior of added noise term for fluorescence

Key insights: - Rrs510-dominant group had the steepest slope (Model 2 & 6) - Fluorescence noise term is credibly nonzero (Model 7) - Posterior variance structure supports heteroscedasticity as a key feature

3.5 3.5 Summary of Bayesian Comparison

- **Model 7**: Best predictive performance (highest ELPD), best uncertainty calibration
- **Model 6**: Nearly equivalent performance; simpler if fluorescence uncertainty not needed
- **Model 2**: Gains from partial pooling; underperforms without variance modeling
- **Model 1**: Legacy structure underfits tails, overconfident predictions

All results support the Bayesian hierarchical modeling framework with heteroscedasticity and measurement-aware noise as optimal for chlorophyll-a estimation.

4 4. Discussion

This section interprets the results in the context of previous chlorophyll-a modeling work, with particular emphasis on the added value of Bayesian modeling. We highlight the importance of accounting for heteroscedasticity and measurement-type uncertainty, and discuss how this contributes to improved predictive reliability and scientific interpretability.

4.1 4.1 Value of Bayesian Framework over Classical Approaches

Our results demonstrate the clear advantages of fully Bayesian modeling for chlorophyll-a prediction from satellite Rrs. Unlike deterministic or frequentist models:

- Bayesian methods explicitly model parameter uncertainty and provide HDIs instead of misleading confidence intervals
- Posterior predictive distributions enable direct evaluation of model calibration
- Bayesian model comparison via LOO-CV avoids overfitting and guards against inappropriate complexity

4.2 4.2 Importance of Hierarchical Structuring

Models that leveraged group-wise structure (based on dominant Rrs bands) consistently outperformed simpler counterparts.

- Hierarchical partial pooling improved both prediction and parameter identifiability
- Group-level trends reflected known biogeophysical distinctions (e.g., clear vs. turbid water types)
- Intercepts and slopes varied systematically across spectral regimes

4.3 4.3 Role of Heteroscedasticity in Chlorophyll Retrieval

Accounting for non-constant noise was essential for accurate uncertainty quantification.

- Models with linear or hierarchical terms captured increased variance at higher MBR or Chl
- Constant- models (e.g., OC6) underrepresented predictive uncertainty, especially in extremes
- Explicit modeling of structure produced calibrated HDIs and superior posterior predictive checks

4.4 4.4 Measurement-Specific Error Modeling

Model 7, which introduced a separate noise term for fluorescence-derived Chl, outperformed all others.

- Fluorescence-based measurements have higher and more variable error
- This heterogeneity cannot be ignored in merged datasets
- Bayesian modeling allows this variance to be encoded explicitly without discarding data

4.5 4.5 Implications for Satellite Algorithm Development

The findings support incorporating Bayesian elements into future operational chlorophyll algorithms.

- Hierarchical modeling offers a path to generalize across bioregions and sensors
- Posterior uncertainty estimates can support downstream applications (e.g., forecasting, ecological thresholds)
- Bayesian frameworks are sensor-agnostic: Rrs inputs can vary as long as priors are adapted

4.6 4.6 Limitations and Future Work

As with any modeling effort, our study has limitations:

- All results are conditional on the data from NOMAD; further validation on independent datasets is needed
- More sophisticated noise structures (e.g., nonparametric) could be explored
- Spatial or spatio-temporal extensions were not considered, but would be feasible in PyMC

5 Acknowledgments

6 Open research

References

Abril-Pla, O., Andreani, V., Carroll, C., Dong, L., Fonnesbeck, C. J., Kochurov, M., et al. (2023). PyMC: A modern, and comprehensive probabilistic programming framework in python. *PeerJ Computer Science*, *9*, e1516. https://doi.org/10.7717/peerj-cs.1516

Baker, M. (2016). 1,500 scientists lift the lid on reproducibility. *Nature*, *533*(7604), 452–454. https://doi.org/10.1038/533452a

Bishop, C. M. (2006). *Pattern recognition and machine learning*. Springer.

Clayton, A. (2022). *Bernoulli's fallacy: Statistical illogic and the crisis of modern science*. Columbia University Press. Retrieved from https://books.google.com/books?id=BT4CzwEACAAJ

Cobey, K. D., Ebrahimzadeh, S., Page, M. J., Thibault, R. T., Nguyen, P.-Y., Abu-Dalfa, F., & Moher, D. (2024). Biomedical researchers' perspectives on the reproducibility of research. *PLoS Biology*, *22*(11), e3002870.

Craig, S. E., & Karaköylü, E. M. (2019). Bayesian models for deriving biogeochemical information from satellite ocean color. *EarthArXiv*. https://doi.org/10.31223/osf.io/shp6y

Erickson, Z. K., McKinna, L. I. W., Werdell, P. J., & Cetinić, I. (2023). Bayesian approach to a generalized inherent optical property model. *Optics Express*, *31*, 22790–22801. https://doi.org/10.1364/oe.486581

Frouin, R., & Pelletier, B. (2013). Bayesian methodology for ocean color remote sensing. Retrieved from https://hal.archives-ouvertes.fr/hal-00822032

Gal, Y. (2016). *Uncertainty in deep learning* (PhD thesis). University of Cambridge.

Hu, C., Lee, Z., & Franz, B. (2012). Chlorophyll aalgorithms for oligotrophic oceans: A novel approach based on three-band reflectance difference. *Journal of Geophysical Research: Oceans*, *117*(C1). https://doi.org/https://doi.org/10.1029/2011JC007395

Hu, C., Feng, L., Lee, Z., Franz, B. A., Bailey, S. W., Werdell, P. J., & Proctor, C. W. (2019). Improving satellite global chlorophyll a data products through algorithm refinement and data recovery. *Journal of Geophysical Research: Oceans*, *124*(3), 1524–1543. https://doi.org/https://doi.org/10.1029/2019JC014941

Jaynes, E. T., & Bretthorst, G. L. (2003). *Probability theory: The logic of science*. Cambridge University Press. Retrieved from https://books.google.com/books?id=tTN4HuUNXjgC

O'Reilly, John E., & Werdell, P. J. (2019). Chlorophyll algorithms for ocean color sensors - OC4, OC5 & OC6. *Remote Sensing of Environment*, *229*, 32–47. https://doi.org/https://doi.org/10.1016/j.rse.2019.04.021

O'Reilly, John E., Maritorena, S., Mitchell, B. G., Siegel, D. A., Carder, K. L., Garver, S. A., et al. (1998). Ocean color chlorophyll algorithms for SeaWiFS. *Journal of Geophysical Research: Oceans*, *103*(C11), 24937–24953. https://doi.org/https://doi.org/10.1029/98JC02160

O'Reilly, John E., Maritorena, S., Siegel, D. A., O'Brien, M. C., Toole, D., Mitchell, B. G., et al. (2000). Ocean color chlorophyll a algorithms for SeaWiFS, OC2, and OC4: Version 4. *SeaWiFS Postlaunch Calibration and Validation Analyses, Part*, *3*, 9–23.

Seegers, B. N., Stumpf, R. P., Schaeffer, B. A., Loftin, K. A., & Werdell, P. J. (2018). Performance metrics for the assessment of satellite data products: An ocean color case study. *Opt. Express*, *26*(6), 7404–7422. https://doi.org/10.1364/OE.26.007404

team, T. pandas development. (2020, February). Pandas-dev/pandas: pandas (Version latest). Zenodo. https://doi.org/10.5281/zenodo.3509134

Vehtari, A., Gelman, A., & Gabry, J. (2017). Practical bayesian model evaluation using leave-one-out cross-validation and WAIC. *Statistics and Computing*, *27*(5), 1413–1432. https://doi.org/10.1007/s11222-016-9696-4

Werdell, P. J., & Bailey, S. W. (2005). An improved bio-optical data set for ocean color algorithm development and satellite data product validation. *Remote Sensing of Environment*, *98*(1), 122–140.